Revista Mexicana de Astronomía y Astrofísica, **60**, 305–316 (2024)

https://doi.org/10.22201/ia.01851101p.2024.60.02.08

RELATIONSHIP BETWEEN PHOTOMETRIC PERIOD AND SURFACE DIFFERENTIAL ROTATION IN CHROMOSPHERICALLY ACTIVE STARS

O. Özdarcan[1], H. A. Dal[1], E. Sipahi Kılıç[1], and E. Yoldaş[1]

Received April 18 2024; accepted June 5 2024

ABSTRACT

We present a quantitative investigation of the relationship between the photometric periods of late-type chromospherically active stars showing spot activity and their photometric period variation interval as the proxy of the surface differential rotation. The results show that as the photometric period increases, the magnitude of the surface differential rotation also increases. However, there is a noticeable distinction between main sequence and evolved stars. Comparing a main sequence star and an evolved star with the same photometric period, it turns out that the magnitude of the surface differential rotation of the main sequence star appears greater than that of the evolved star. The distinction is apparent around short photometric periods but tends to disappear towards longer photometric periods.

RESUMEN

Presentamos una investigación cuantitativa de la relación entre los períodos fotométricos de estrellas tardías con actividad cromosférica y manchas y el intervalo de variación del período fotométrico, como indicador de la rotación diferencial superficial. Los resultados muestran que al aumentar el período fotométrico aumenta también la magnitud de la rotación diferencial superficial. Sin embargo, hay una diferencia notable entre estrellas de la secuencia principal y estrellas evolucionadas. Al comparar ambas, encontramos que la magnitud de la rotación diferencial superficial es mayor en las estrellas de la secuencia principal que en las evolucionadas, para períodos fotométricos iguales. Esta diferencia es notable para los períodos fotométricos cortos pero tiende a desaparecer hacia períodos mayores.

Key Words: stars: activity — stars: late-type — stars: rotation

1. INTRODUCTION

The most comprehensive and long-term study to investigate chromospheric activity in stars is the Mount Wilson HK project, which started in 1966 and continued for almost 40 years until 2003 (Wilson 1978; Vaughan et al. 1978; Duncan et al. 1991; Baliunas et al. 1995). The HK project aimed to examine the chromospheric activity and its change in stars by measuring the resonance doublet of singly ionized calcium (Ca II H& K), which is a good indicator of chromospheric activity. From the long-term Ca II H& K measurements, it was found that 60% of the observed stars exhibited periodic and cyclical changes similar to the solar activity cycle (Baliunas et al. 1998). Donahue et al. (1996) applied period analysis to the 12-year HK measurements of 37 main sequence stars observed within the scope of the HK project and determined the largest (P_{max}) and the smallest (P_{min}) values of the observed photometric periods of each star. They also calculated the $\Delta P = P_{max} - P_{min}$ values and the average photometric period of each star determined over 12 years and adopted this value as the average rotation period ($\overline{P}$) of the relevant star. When they plotted the calculated ΔP and $\overline{P}$ against each other on a logarithmic scale, they found a linear relationship showing that as the $\overline{P}$ increased, the ΔP also increased. A similar study was conducted by Messina & Guinan (2003), who analysed the long-term photometry of 14 main sequence stars, and they found the linear relationship between ΔP and the $\overline{P}$. The advent of unprecedented $KEPLER$ photometry enabled scientists to focus on the relationship between ΔP and $\overline{P}$ over a very large sample. Based on the ex-

[1]Department of Astronomy and Space Sciences, Faculty of Science, Ege University, 35100, İzmir, Turkey.

tremely precise *KEPLER* data, Reinhold & Gizon (2015) analysed four years of continuous photometry of 12 319 stars and confirmed the linear relationship between the aforementioned quantities. The only restriction of their study is that the observations span over only four years. In chromospherically active stars, cool surface spots may emerge from different latitudes at different times; therefore, long-term continuous photometric observations become crucial to increase the detection chance of surface spots emerging from a wider latitude range. Taking this into consideration, Özdarcan (2021) conducted a comprehensive spectroscopic and photometric review of 21 chromospherically active stars. They adopted $\Delta P/P_{min}$ as a measure of the surface differential rotation (SDR), instead of ΔP. They established a quantitative linear relationship between $\Delta P/P_{min}$ and P_{min}. They implicitly assumed that the target stars possess solar-type differential rotation and hence P_{min} practically corresponds to the equatorial rotation period. Moreover, they noticed a suspicious separation between main sequence stars and giant stars. According to this separation, it was concluded that the photometric period of giant stars is closely related to the SDR, but in main sequence stars, this relationship is slightly weaker than what is observed in giants. Kővári et al. (2017) showed that binarity may play a critical role in the observed strength of SDR and hence might be responsible for the observed photometric period – relative shear distribution.

Rechecking the results given in Özdarcan (2021) with a larger sample group will provide information about the reliability of the separation and enable the relationship between the rotation period and the SDR to be determined more reliably over a broader range of photometric periods. For this purpose, thirty-five stars that were determined to show chromospheric activity and have never been studied before, were selected. In the next section, we describe new observations and collected data of the target stars. In the third section, we estimate the astrophysical properties of the target stars from new UBV observations and determine seasonal photometric periods from long-term photometry to estimate the magnitude of the surface differential rotation. In the final section, we summarize our findings and give a comparison with theoretical predictions.

2. DATA

2.1. *Observations*

We carry out Johnson UBV observations of the target stars with a 0.35m Schmidt-Cassegrain telescope equipped with Optec SSP-5 photometer located at Ege University Observatory Application and Research Center (EUOARC). The photometer includes an R6358 photomultiplier tube, which is sensitive to the longer wavelengths at the optical part of the electromagnetic spectrum. We use a circular diaphragm with an angular size of $53''$ and we adopt ten seconds of integration time for all observations. A typical observing sequence for a selected target is like sky-sky-VAR-VAR-VAR-VAR-sky-sky, where sky and VAR denote measurements from the sky and the variable star, respectively. We list the target stars in Table 1.

We follow the procedure described in Hardie (1964) to obtain reduced instrumental magnitudes. Moreover, we observe a set of standard stars selected from Landolt (2009) and Landolt (2013) along with each target. Hence, we transform all reduced instrumental magnitudes of the target stars into the standard system. Since RA coordinates of the target stars are distributed homogeneously around the celestial equator, we carried out standard star observations on two nights with an almost six-month time difference. These are 27th December 2022 and 13th July 2023 nights. We give computed transformation coefficients in the Appendix section.

Preliminary analysis of the EUOARC observations shows that signal-to-noise ratios of TYC 5275-00646-1, V1330 Sco, TYC 5610-00066-1, TYC 5050-00802-1, TYC 01572-00794-1 and GSC 00140-01925 are not sufficient for reliable colour and magnitude measurements. Increasing the integration time or gain, or using another EUOARC telescope (0.4m Schmidt-Cassegrain with a CCD camera and standard Johnson–Bessell filters) does not change the situation. Therefore, we take $B-V$ colours and V magnitudes of these stars from The AAVSO Photometric All-Sky Survey for analysis (APASS; Henden et al. 2015). We tabulate standard colours and magnitudes of the target systems in Table 2.

2.2. *Long-Term Photometry*

Besides EUOARC observations, we collect long-term V photometry of target stars from The All Sky Automated Survey (ASAS, Pojmanski 1997, 2002; Pojmanski et al. 2005) and All-Sky Automated Survey for Supernovae Sky Patrol (ASAS-SN, Shappee et al. 2014; Kochanek et al. 2017). The time range of the collected data usually spans over 15 or 18 years, depending on the beginning and the end of the observations. However, there is a significant time gap (3 or 4 years) between ASAS and ASAS-SN data, where no observation is available. This prevents us from precise tracing of the long-term photometric behaviour of our target systems. These time gaps are

TABLE 1

LIST OF TARGET STARS

Target Star	GCVS Identifier	RA (2000) (h m s)	Dec (2000) (° ′ ″)	V (mag)	$B-V$ (mag)	Ref.
TYC 05275-00646-1	IM Cet	01 01 45.3	−12 08 02.4	9.67	1.042	3
TYC 04688-02015-1	IR Cet	01 46 51.7	−05 47 15.1	11.29	1.37	7
TYC 05282-02210-1	IZ Cet	02 19 47.3	−10 25 40.6	10.72	1.076	2
TYC 00648-01252-1	HW Cet	03 12 34.2	+09 44 57.1	10.39	1.089	1
TYC 04723-00878-1	LN Eri	03 48 36.2	−05 20 30.4	11.713	0.971	5
TYC 04734-00020-1	OP Eri	04 36 12.5	−01 50 24.9	10.17	0.961	7
TYC 00083-00788-1	V1330 Tau	04 42 18.5	+01 17 39.8	11.88	1.042	1
V1339 Tau	V1339 Tau	04 48 57.9	+19 14 56.1	11.8	1.141	1
TYC 01281-01672-1	V1841 Ori	05 00 49.2	+15 27 00.6	10.83	1.218	1
TYC 00099-00166-1	V1854 Ori	05 13 19.0	+01 34 47.0	10.28	0.907	1
TYC 04767-00071-1	V2814 Ori	05 39 45.6	−00 55 51.0	11.33	1.212	7
GSC 00140-01925	V2826 Ori	06 15 18.6	+03 47 01.0	11.64	1.483	7
TYC 04806-03158-1	V969 Mon	06 36 56.3	−05 21 03.6	11.71	0.66	2
TYC 01358-01303-1	V424 Gem	07 16 50.4	+21 45 00.1	10	1.074	1
TYC 01942-00318-1	KU Cnc	08 35 26.8	+24 15 39.4	11.48	1.201	1
TYC 00840-00219-1	EQ Leo	10 13 23.8	+12 08 45.7	9.345	1.091	1
TYC 00845-00981-1	IN Leo	10 39 59.0	+13 27 22.0	10.326	0.901	1
TYC 00856-01223-1	OS Leo	11 33 36.9	+07 51 28.9	11.369	1.344	6
TYC 00865-01164-1	V358 Vir	11 56 51.6	+08 27 21.3	11.37	1.347	1
TYC 00881-00657-1	PW Com	12 35 57.4	+13 29 25.2	10.27	1.044	2
TYC 05003-00309-1	V436 Ser	15 23 46.1	−00 44 24.7	11.13	1.214	1
TYC 05003-00138-1	V561 Ser	15 26 52.7	−00 53 11.7	11.39	1.201	7
TYC 05610-00066-1	V354 Lib	15 54 44.9	−07 52 04.5	11.34	1.229	1
V1330 Sco	V1330 Sco	16 23 07.8	−23 00 59.9	11.85	1.263	1
TYC 05050-00802-1	V2700 Oph	16 51 22.1	−00 50 01.2	11.7	1.007	5
TYC 00990-02029-1	V1404 Her	17 16 29.7	+13 23 14.5	11.41	0.758	7
GSC 00978-01306	V2723 Oph	17 17 11.4	+08 15 24.6	12	1	4
TYC 01572-00794-1	V1445 Her	18 16 52.7	+17 57 03.1	11.22	0.726	7
TYC 01062-01972-1	V1848 Aql	19 54 03.1	+10 41 45.4	10.16	0.965	6
TYC 05165-00365-1	V1890 Aql	20 11 39.5	−02 35 25.7	11.15	0.975	7
TYC 05183-00044-1	V365 Aqr	20 54 09.2	−02 45 33.7	10.74	0.964	7
GSC 00563-00384	V641 Peg	22 28 36.1	+03 05 25.6	11.89	1.165	7
TYC 02221-00759-1	V543 Peg	22 47 22.7	+23 13 16.6	11.48	1.197	7
TYC 01712-00736-1	V580 Peg	23 12 29.0	+17 09 21.7	11.107	1.467	1
TYC 00583-00566-1	KZ Psc	23 16 45.0	+06 18 57.4	10.77	1.027	7

References are 1: Berdnikov & Pastukhova (2008), 2: Bernhard & Otero (2011), 3: Bernhard et al. (2009), 4: Bernhard & Lloyd (2008b), 5: Bernhard & Lloyd (2008a), 6: Bernhard et al. (2010), 7: Schirmer et al. (2009). V and $B-V$ magnitudes are from Tycho catalogue (Høg et al. 2000).

filled with unpublished observations obtained in the scope of the extension of the ASAS project (ASAS3-N and ASAS4; Pojmanski, 2022; priv. comm.). Therefore, we are able to collect photometric data of the target stars without a significant time gap. We plot the collected data of each target in Figure 1.

3. ANALYSIS

3.1. *Photometric Properties*

In the first step of our analysis, we plot measured standard $U-B$ and $B-V$ colours of the target systems in a colour – colour diagram (Figure 2). More than half of the target stars appear systematically shifted from the predicted positions of the unreddened main sequence stars. This could be interpreted as the effect of interstellar reddening, which means a kind of systematic interstellar reddening is valid for most of our target stars. However, these stars are located at different positions in the celestial sphere. If one applied a reddening correction suggested by Figure 2, then many of the target stars would become early-type stars. This is contradictory to the reported properties of our tar-

TABLE 2

JOHNSON UBV STANDARD MAGNITUDES AND COLOURS OF THE TARGET SYSTEMS

Star	V (mag)	σ_V (mag)	$B-V$ (mag)	σ_{B-V} (mag)	$U-B$ (mag)	σ_{U-B} (mag)	$E(B-V)$ (mag)	$(B-V)_0$ (mag)
IM Cet *	10.38	0.05	1.10	0.10	—	—	0.0275	1.16
IR Cet	11.39	0.06	1.09	0.09	0.54	0.29	0.0228	1.16
IZ Cet	10.25	0.06	1.01	0.06	0.77	0.19	0.0242	1.08
HW Cet	10.77	0.05	0.99	0.02	0.81	0.15	0.3132	0.77
LN Eri	11.79	0.05	1.02	0.05	−0.06	0.13	0.0787	1.03
OP Eri	10.13	0.06	1.05	0.04	0.58	0.14	0.0422	1.10
V1330 Tau	11.71	0.06	1.16	0.13	0.51	0.20	0.1144	1.14
V1339 Tau	11.99	0.07	1.02	0.07	1.11	0.30	0.4134	0.70
V1841 Ori	11.06	0.06	1.24	0.04	1.19	0.45	0.3542	0.98
V1854 Ori	10.37	0.05	0.92	0.04	0.27	0.16	0.1111	0.90
V2814 Ori	11.19	0.08	1.52	0.07	1.81	0.17	0.3338	1.28
V2826 Ori *	11.64	0.05	1.48	0.08	—	—	0.6493	0.92
V969 Mon	11.53	0.08	1.37	0.09	1.03	0.39	0.3963	1.06
V424 Gem	10.38	0.06	1.19	0.02	1.08	0.18	0.0559	1.22
KU Cnc	11.59	0.11	1.38	0.11	1.96	0.38	0.0276	1.44
EQ Leo	9.56	0.06	1.19	0.03	0.79	0.17	0.0326	1.25
IN Leo	10.55	0.06	1.01	0.07	0.41	0.17	0.0339	1.07
OS Leo	11.71	0.06	0.98	0.06	0.00	0.19	0.0380	1.03
V358 Vir	11.58	0.06	1.00	0.04	0.73	0.35	0.0165	1.07
PW Com	10.55	0.05	0.79	0.06	0.09	0.17	0.0308	0.85
V436 Ser	11.32	0.15	1.12	0.19	0.53	0.61	0.0485	1.16
V561 Ser	11.35	0.16	1.17	0.19	0.57	0.48	0.0557	1.20
V354 Lib *	11.38	0.06	1.16	0.10	—	—	0.1607	1.09
V1330 Sco *	11.85	0.04	1.26	0.07	—	—	1.8802	1.35
V2700 Oph *	11.72	0.17	1.28	0.22	—	—	0.1014	1.27
V1404 Her	11.78	0.20	0.91	0.25	0.64	0.31	0.1403	0.86
V2723 Oph	12.24	0.20	1.10	0.28	0.32	0.29	0.1047	1.09
V1445 Her *	11.18	0.12	0.98	0.15	—	—	0.1865	0.88
V1848 Aql	10.07	0.10	0.97	0.08	0.35	0.24	0.2900	0.77
V1890 Aql	11.17	0.12	1.26	0.18	0.08	0.27	0.1631	1.19
V365 Aqr	10.91	0.23	0.82	0.26	0.83	0.34	0.0783	0.83
V641 Peg	11.69	0.08	1.07	0.14	−0.15	0.23	0.0824	1.08
V543 Peg	11.38	0.07	0.88	0.14	0.67	0.36	0.0847	0.89
V580 Peg	11.05	0.08	1.27	0.12	0.91	0.25	0.1112	1.25
KZ Psc	10.59	0.09	1.17	0.14	0.48	0.23	0.0773	1.18

Note: V and $B-V$ measurements of the target stars (marked by * sign) are from Henden et al. (2015). These targets do not have reliable U measurement. In the last two columns, we list the estimated interstellar reddening values and corrected $B-V$ colour indexes. See text for the details.

get stars, such as detected X-ray emission, photometric colours and light curve properties (see references mentioned in Table 1). In this case, interstellar reddening cannot be a satisfactory explanation for the disagreement between observed and predicted colours seen in Figure 2. An alternative explanation is colour excess due to the chromospheric activity of the target stars. Since their chromospheric activity was confirmed by their properties in the references mentioned above, we may expect average colour excesses of $0\overset{\mathrm{m}}{.}09$ and $0\overset{\mathrm{m}}{.}35$ for $B-V$ and $U-B$ colours, respectively (Amado 2003). Due to these colour excesses, the observed $U-B$ and $B-V$ colours become bluer than their predicted values from standard stellar atmosphere models. An observational test of the suggested colour excess was done for the observed colours of HD 208472, an RS CVn variable, and corrected colours indicated an effective temperature, which was in agreement with spectroscopically estimated one (Özdarcan et al. 2010). To calculate reliable astrophysical parameters of the target stars, we aim to remove the effects of both interstellar reddening and activity-originated colour excess from the observed $B-V$ colours. Regarding interstellar red-

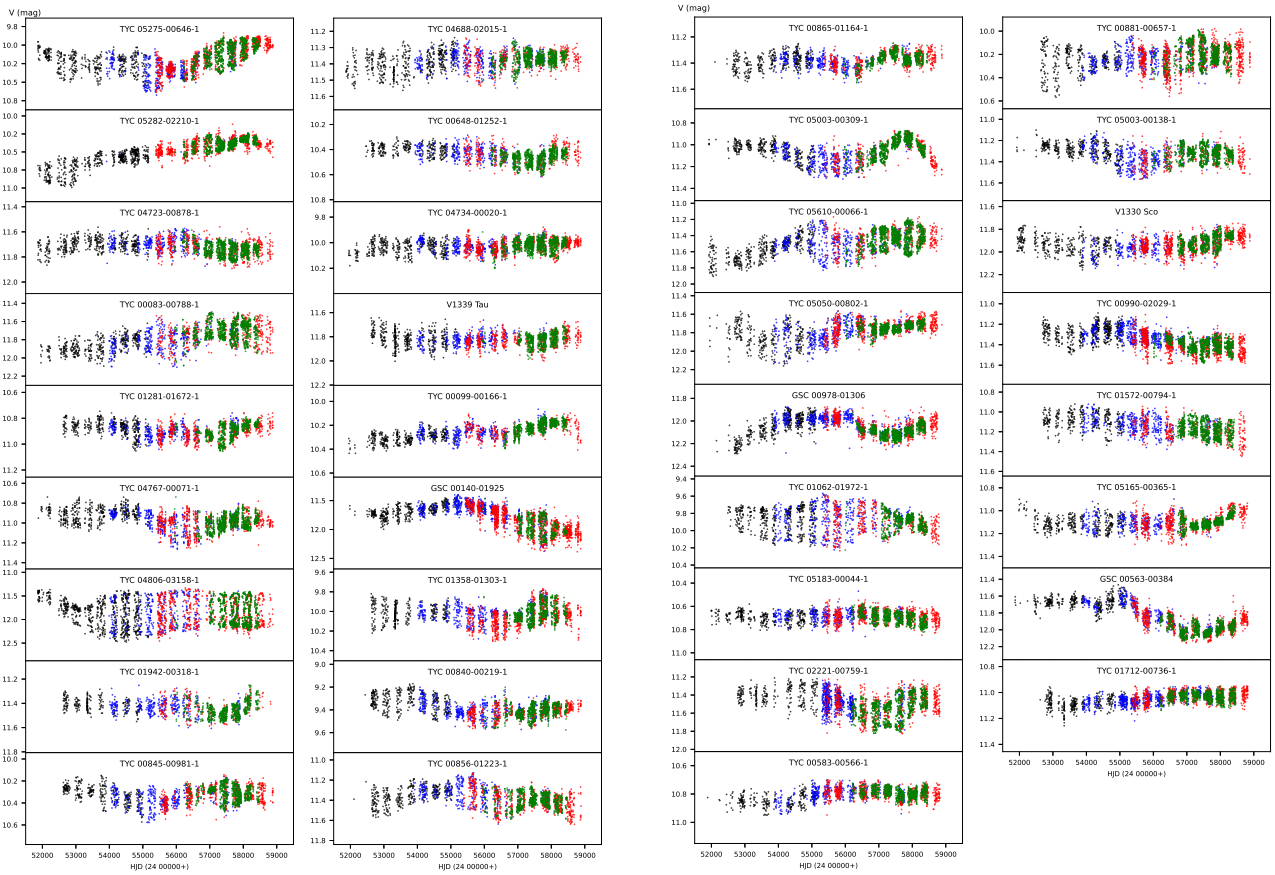

Fig. 1. Compiled ASAS3 (black), ASAS3-N (blue), ASAS4 (red) and and ASAS-SN (green) photometry of target stars. The colour figure can be viewed online.

dening, we adopt the estimated mean $E(B-V)$ colour excess (Schlafly & Finkbeiner 2011) for the precise equatorial coordinates of each target. Then, we subtract the estimated $E(B-V)$ excess from the observed $B-V$ colour (fourth column in Table 2). For correction of activity-originated average blue excess in $B-V$ colour, we add $0\overset{\mathrm{m}}{.}09$ to each reddening corrected $B-V$ colour and obtain the final $B-V$ colour index of each target. We list the estimated $E(B-V)$ values and corrected $B-V_0$ colour index of each target in the last two columns of the Table 2. Here, we note that we find unreasonably large reddening for V1330 Sco ($E(B-V) \approx 1\overset{\mathrm{m}}{.}88$) from Schlafly & Finkbeiner (2011). Using this correction, we find a hot (≈ 25000 K) main sequence star. This finding is not consistent with the previously reported properties of the star (see reference given in Table 1). Therefore, we omit the effect of interstellar reddening for this star and only apply the activity-related $0\overset{\mathrm{m}}{.}09$ colour excess correction to the observed $B-V$ colour index.

3.2. *Astrophysical Properties*

By using the corrected $B-V$ colours, we first determine the effective temperatures (T_{eff}) and bolometric corrections (BC) of the target stars according to the empirical colour – temperature and colour – bolometric correction relations given in Gray (2005). Then, we determine the distance of each target depending on its parallax measurement taken from the third GAIA data release (Gaia Collaboration et al. 2016, 2023). In the third step, we use the measured V magnitudes (in Table 2) and the calculated distances (d) of each target in the distance modulus formula and find the absolute V magnitude (M_V). After that, we apply estimated bolometric corrections to the calculated M_V magnitudes and obtain the bolometric absolute magnitude (M_{bol}) of each star. In the final step, we use the calculated M_{bol} of each star with the solar M_{bol} value of $4\overset{\mathrm{m}}{.}74$ in Stefan-Boltzmann law and calculate the luminosity ($L/L_{\odot}$) of the target stars. We estimate the spectral clas-

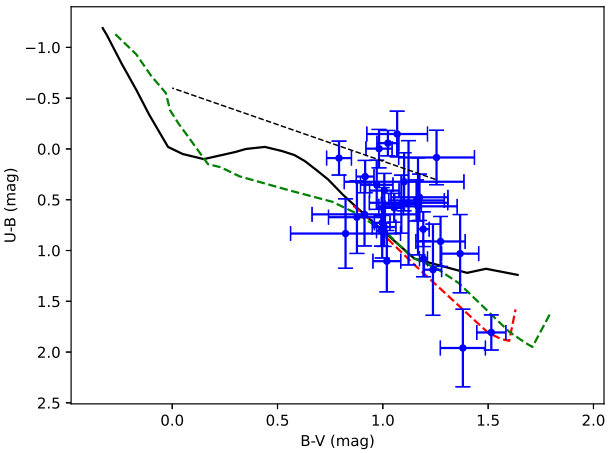

Fig. 2. Positions of the target systems on the UBV colour – colour diagram. Six targets that do not have reliable measurements are not plotted in the figure. The continuous curve (black) shows the theoretically expected positions of the unreddened main sequence stars, while the dashed curves show the positions of unreddened giant (shorter curve) and supergiant stars (longer curve), respectively. The dashed (black) line denotes the reddening vector. Theoretical data are from Drilling & Landolt (2000). The colour figure can be viewed online.

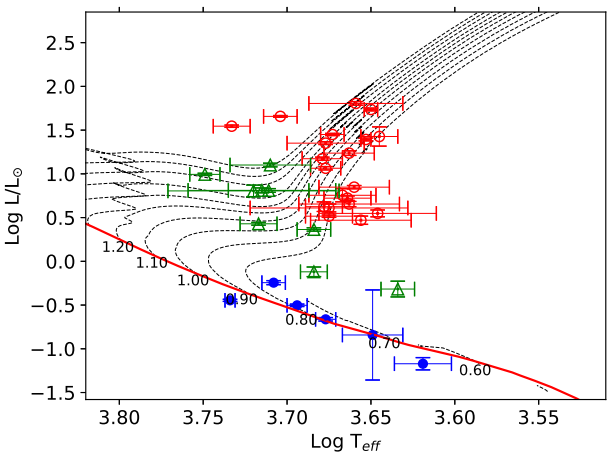

Fig. 3. Positions of the target systems on the HR diagram. Theoretical evolutionary tracks (dashed lines) for solar abundance ($Y = 0.279$ and $Z = 0.017$) are from Bressan et al. (2012). Each track is labelled with its corresponding mass in solar units. Continuous (red) curve denotes the zero-age main sequence. Filled (blue) circles are for main sequence stars, open triangles (green) denote sub-giant stars and open (red) circles show giant stars. The colour figure can be viewed online.

sification of each star by comparing estimated effective temperatures and calculated luminosities with the calibrations given in Gray (2005). Following the outlined procedure, we calculate the results listed in Table 3.

Now, we are in a position to determine the location of each target on the Hertzsprung – Russell (HR) diagram (Figure 3). In the figure, one may notice that there is no available evolutionary track for the positions of a few targets located at the redder part of the diagram. These targets may be pre-main sequence stars, which still evolve towards the zero-age main sequence. LN Eri, V1330 Sco, V2700 Oph and KZ Psc might be pre-main sequence stars with their remarkably short photometric periods ($P < 8$ day) and a light curve amplitude between $0\overset{\mathrm{m}}{.}1$ or $0\overset{\mathrm{m}}{.}2$ in the V filter (see Table 5 in the Appendix). Optical spectroscopic observations of these particular targets are required to arrive at a conclusive result.

3.3. *Analysis of Seasonal Light Curves*

We use long-term photometry of each star (Figure 1) to determine seasonal light curve properties, which are photometric period (P_{phot}), peak-to-peak light curve amplitude (A) and minimum (V_{min}), maximum (V_{max}) and mean (V_{mean}) brightnesses. For that purpose, we first divide the photometric data of a given target into subsets, where each one covers an observing season. Then, we check each season by eye for any dramatic change in light curve amplitudes. If there is a significant amplitude change in a season, we further divide the corresponding subset into parts so that each part possesses a fairly constant amplitude.

Among photometric period determination methods, we employ Analysis of Variance (ANOVA, Schwarzenberg-Czerny 1996), which is a hybrid method that combines the power of Fourier analysis and ANOVA statistics. The method is capable of determining the best-fitting period for a given light curve independently of the shape of the light curve and is very effective to damp the amplitudes of the alias periods[2]. To estimate the uncertainty of the computed photometric periods, we follow the method proposed by Schwarzenberg-Czerny (1991). The method provides more accurate uncertainties compared to the least-squares correlation matrix or Rayleigh resolution criteria.

Before proceeding with the ANOVA method, we apply a linear fit to the corresponding subset light curve to remove any long-term brightness variation, because such a variation may alter the photomet-

[2]Practical application of the method is done by computer codes/scripts located at `https://users.camk.edu.pl/alex/\#software`

TABLE 3

ESTIMATED ASTROPHYSICAL PROPERTIES OF THE TARGET STARS

Star	T_{eff} (K)	$\sigma_{T_{eff}}$ (K)	BC (mag)	d (pc)	σ_d (pc)	M_V (mag)	σ_{M_V} (mag)	M_{bol} (mag)	$\sigma_{M_{bol}}$ (mag)	$L/L_\odot$	$\sigma_{L/L_\odot}$	Sp.
IM Cet	4602	161	-0.495	427	7	2.14	0.19	1.65	0.10	17	1	K2 III
IR Cet	4610	150	-0.492	379	2	3.43	0.10	2.93	0.06	5.3	0.3	K2 III
IZ Cet	4752	99	-0.430	341	3	2.51	0.10	2.08	0.05	11.6	0.5	K1 III
HW Cet	5415	41	-0.149	57.4	0.1	6.00	0.05	5.86	0.07	0.36	0.01	G9 V
LN Eri	4834	91	-0.391	167	4	5.43	0.31	5.04	0.15	0.76	0.09	K0 IV
OP Eri	4713	75	-0.448	486.62	0.09	1.56	0.06	1.11	0.03	28.2	0.8	K1 III
V1330 Tau	4647	212	-0.477	403	14	3.33	0.41	2.85	0.23	5.7	0.9	K1 III
V1339 Tau	5608	116	-0.103	468	5	2.36	0.14	2.25	0.07	9.9	0.3	G1 IV
V1841 Ori	4941	63	-0.339	53.09	0.04	6.34	0.06	6.00	0.08	0.31	0.01	K3 V
V1854 Ori	5101	81	-0.264	76.3	0.8	5.61	0.13	5.35	0.08	0.57	0.03	K2 V
V2814 Ori	4417	106	-0.563	483	5	1.74	0.14	1.17	0.23	27	6	K3 III
V2826 Ori	5054	118	-0.285	561	1	0.88	0.06	0.60	0.08	45	1	G6 III
V969 Mon	4774	133	-0.420	412	3	2.23	0.11	1.81	0.10	14.9	0.6	K0 III
V424 Gem	4500	30	-0.533	482	2	1.79	0.07	1.26	0.04	24.7	0.9	K2 III
KU Cnc	4163	162	-0.760	41.27	0.03	8.43	0.11	7.67	0.12	0.07	0.01	M1 V
EQ Leo	4463	44	-0.546	504	3	0.95	0.09	0.40	0.05	54	2	K3 III
IN Leo	4769	124	-0.422	234	6	3.60	0.31	3.18	0.14	4.2	0.5	K1 III
OS Leo	4832	112	-0.392	298	2	4.22	0.09	3.83	0.06	2.3	0.1	K0 IV
V358 Vir	4756	66	-0.429	87.2	0.2	6.83	0.06	6.40	0.07	0.22	0.01	K4 V
PW Com	5213	132	-0.217	206	1	3.89	0.09	3.67	0.05	2.7	0.1	G4 IV
V436 Ser	4603	307	-0.495	326.9	0.4	3.60	0.15	3.10	0.09	4.5	0.3	K2 III
V561 Ser	4532	299	-0.521	262	2	4.09	0.18	3.56	0.11	3.0	0.3	K2 III
V354 Lib	4728	155	-0.442	250.1	0.4	3.89	0.07	3.45	0.06	3.3	0.1	K1 III
V1330 Sco	4303	101	-0.619	138	4	6.15	0.31	5.53	0.20	0.48	0.09	K4 IV
V2700 Oph	4429	342	-0.559	313	1	3.93	0.17	3.37	0.12	3.5	0.3	K3 III
V1404 Her	5188	497	-0.227	480	2	2.94	0.20	2.71	0.08	6.5	0.4	G4 IV
V2723 Oph	4735	485	-0.438	449	4	3.65	0.22	3.22	0.12	4.1	0.4	K1 III
V1445 Her	5135	276	-0.249	337	2	2.96	0.13	2.71	0.07	6.5	0.3	G5 IV
V1848 Aql	5407	141	-0.151	425	5	1.03	0.16	0.88	0.07	35	1	G2 III
V1890 Aql	4561	280	-0.511	967	4	0.74	0.13	0.23	0.08	64	3	K2 III
V365 Aqr	5254	580	-0.202	353	18	2.93	0.63	2.73	0.18	6.4	0.9	G4 IV
V641 Peg	4749	245	-0.432	847	2	1.80	0.08	1.36	0.05	22.4	0.8	K1 III
V543 Peg	5131	274	-0.251	597	8	2.24	0.16	1.99	0.06	12.6	0.6	G5 III
V580 Peg	4461	180	-0.547	46	6	7.39	1.53	6.84	0.97	0.1	0.1	K6 V
KZ Psc	4568	215	-0.508	278.22	0.05	3.13	0.09	2.62	0.06	7.0	0.3	K2 III

ric period artificially. After the linear correction, we apply the ANOVA method to the residuals from the linear fit and determine the best-fitting period and the light curve properties mentioned above. After we find the final photometric period for a given subset, we make a phase-folded light curve of this subset concerning the final photometric period and fit a cubic spline polynomial to the phase-folded data. Here, the purpose is to determine the minimum and the maximum values of the spline function, which correspond to the brightnesses of the light curve maximum and minimum, respectively. The amplitude and the mean brightness can be calculated straightforwardly from these values. Otherwise, fitted spline polynomials do not have any physical meaning. We list the analysis results in the Appendix (Table 5).

3.4. *Photometric Periods and Surface Differential Rotation*

In this section, we use the advantage of having long-term photometry to estimate the magnitude of the SDR. It is clear that determining the latitude of the cool surface spots from photometry is a well-known ill-posed problem. This prevents the type of differential rotation (solar type or anti-solar type) from being clearly determined in this study. However, the range in which the photometric period takes value for a particular star can set a lower limit for

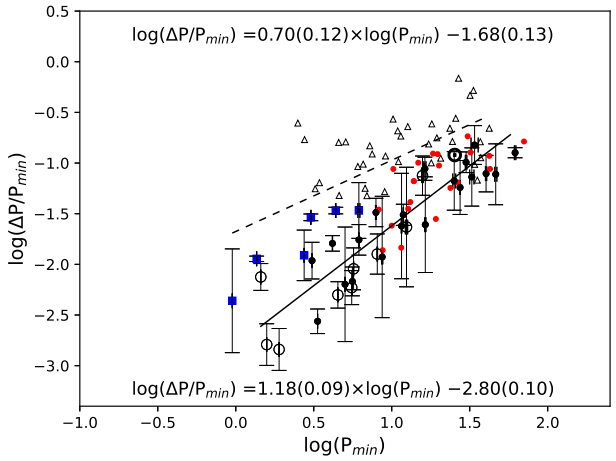

Fig. 4. Relation between the observed minimum period P_{min} and the calculated relative shear. Black filled circles show giant stars listed in Table 5, while blue filled square and open circle symbols denote main sequence stars and sub-giant stars, respectively. Open triangles show stars taken from Donahue et al. (1996), small (red) dots (without error bars) show RS CVn stars analysed in Özdarcan (2021) and five other stars mentioned in the text. We also show the position of our Sun in the figure. Dashed and straight lines show linear fits to the distribution of main sequence and giant stars, respectively. The corresponding coefficients and their statistical errors are given inside the plot window (upper one for the main sequence stars, lower one for the giant stars). The colour figure can be viewed online.

the magnitude of the SDR. Given the brief discussion above, we implicitly assume that all target stars possess solar-type SDR (i.e., the equator rotates faster than the poles). Therefore, we consider the observed minimum value of the photometric period as the equatorial rotation period. The observed maximum value, then, corresponds to the highest latitude at which spots could emerge during the time interval of the photometric data. We make a quantitative estimation of the magnitude of the SDR by relative shear defined in terms of periods (equation 1),

$$\frac{\Delta P}{P_{min}} = \frac{(P_{max} - P_{min})}{P_{min}}. \qquad (1)$$

We take P_{max} and P_{min} values of each target star from Table 5 and compute the relative shear via equation 1. We plot the P_{min} – relative shear pair of each star in Figure 4. We also tabulate these pairs along with the estimated spectral types in Table 4.

For comparison, we also show the positions of the 37 main sequence stars analysed in Donahue et al. (1996) and 21 giant stars analysed in Özdarcan (2021). Five more giant stars are also plotted in the figure (with red dots), which are HD 208472 (Özdarcan et al. 2010), FG UMa (HD 89546, Özdarcan et al. 2012) and BD+13 50000, TYC 5163-1764-1 and BD+11 3024 (Özdarcan & Dal 2018). We note that analysis of all these stars was done in a similar way as described above. The only difference could be that Donahue et al. (1996) used the S index based on Ca II H& K measurements, which is a spectroscopic indicator of the chromospheric activity. For the remaining stars, pure V photometry, which is a photometric indicator of the same phenomenon, was used.

A linear fit to the positions of all main sequence stars plotted in Figure 4 gives the coefficients shown in the upper part of the figure with a correlation coefficient of 0.67 and a p value of 6.9×10^{-7}. In the figure, sub-giants and giants appear as aligned on the same slope. Thus, we apply a similar linear fit to the positions of all giant and sub-giant stars. The fit results in the coefficients shown in the bottom part of the figure with a correlation coefficient of 0.88 and a p value of 3.2×10^{-19}.

4. SUMMARY AND DISCUSSION

Johnson UBV photometry of 35 target stars suggests a significant colour excess, particularly in the $U - B$ colour, for most of the targets. We interpret this excess as the effect of intense chromospheric activity in the UBV colours. Neglecting the interstellar reddening, adopting average $B - V$ colour excess reported in Amado (2003) and using GAIA parallaxes, we estimate astrophysical properties of the target stars via colour-temperature calibrations. At that point, we stress that we remove an average excess value from our observations, which apparently reduces the reliability of the estimated astrophysical properties. Therefore, we believe that a re-determination of colour excesses in $U - B$ and $B - V$ colours with a more comprehensive study based on a larger sample size deserves effort. In the current case, the positions of the target stars on the HR diagram indicate that six of our target stars are main-sequence star, while nine of them appear as sub-giant, and the remaining 20 stars are located in the region of giant stars.

Analysis of long-term V photometry of the target stars enables us to investigate possible variability of the photometric period, which indicates SDR. We determine seasonal photometric periods of each star and calculate the relative shear via observed minimum and maximum photometric periods in the time span of the available photometric data. However, among stars which we classify as giant, we find

TABLE 4

CALCULATED PERIODS AND RELATIVE SHEAR VALUES OF THE TARGET STARS ALONG WITH THEIR SPECTRAL TYPES

Star	Sp.	P_{min} (day)	$\sigma_{P_{min}}$ (day)	P_{max} (day)	$\sigma_{P_{max}}$ (day)	$\Delta P/P_{min}$	$\sigma_{\Delta P/P_{min}}$
IM Cet	K2 III	27.4	0.2	29.0	0.7	0.06	0.03
IR Cet	K2 III	16.3	0.3	17.7	0.2	0.09	0.02
IZ Cet	K1 III	7.92	0.06	8.18	0.04	0.032	0.009
HW Cet	G9 V	6.15	0.09	6.36	0.03	0.03	0.02
LN Eri	K0 IV	1.4467	0.0009	1.458	0.003	0.008	0.002
OP Eri	K1 III	46.4	0.8	50	2	0.08	0.04
V1330 Tau	K1 III	8.68	0.08	8.787	0.005	0.012	0.009
V1339 Tau	G1 IV	15.7	0.2	16.9	0.4	0.08	0.03
V1841 Ori	K3 V	2.743	0.009	2.78	0.01	0.012	0.005
V1854 Ori	K2 V	1.3609	0.0007	1.3764	0.0006	0.0113	0.0007
V2814 Ori	K3 III	61.8	0.7	69.6	0.5	0.13	0.01
V2826 Ori	G6 III	25.2	0.5	26.8	0.6	0.07	0.03
V969 Mon	K0 III	5.018	0.006	5.05	0.02	0.006	0.005
V424 Gem	K2 III	40.2	0.4	43	1	0.08	0.03
KU Cnc	M1 V	0.950	0.001	0.954	0.005	0.004	0.006
EQ Leo	K3 III	33	1	35.0	0.5	0.07	0.04
IN Leo	K1 III	6.161	0.009	6.27	0.03	0.017	0.005
OS Leo	K0 IV	5.69	0.01	5.74	0.01	0.009	0.003
V358 Vir	K4 V	4.376	0.007	4.525	0.009	0.034	0.002
PW Com	G4 IV	4.514	0.004	4.537	0.004	0.005	0.001
V436 Ser	K2 III	11.55	0.06	11.8	0.4	0.02	0.03
V561 Ser	K2 III	11.86	0.01	12.22	0.08	0.031	0.007
V354 Lib	K1 III	5.594	0.002	5.63	0.01	0.007	0.002
V1330 Sco	K4 IV	8.08	0.04	8.18	0.01	0.013	0.005
V2700 Oph	K3 III	3.347	0.002	3.356	0.001	0.003	0.001
V1404 Her	G4 IV	12.4	0.2	12.72	0.04	0.02	0.02
V2723 Oph	K1 III	3.08	0.01	3.116	0.003	0.011	0.004
V1445 Her	G5 IV	1.896	0.001	1.8986	0.0002	0.001	0.001
V1848 Aql	G2 III	16.4	0.2	16.8	0.2	0.02	0.02
V1890 Aql	K2 III	34	2	39.1	0.5	0.15	0.05
V365 Aqr	G4 IV	1.5789	0.0004	1.5814	0.0009	0.002	0.001
V641 Peg	K1 III	30.0	0.3	33.0	0.5	0.10	0.02
V543 Peg	G5 III	5.538	0.005	5.571	0.009	0.006	0.002
V580 Peg	K6 V	3.030	0.006	3.119	0.003	0.029	0.002
KZ Psc	K2 III	4.168	0.009	4.235	0.006	0.016	0.003

very short rotation periods. V2723 Oph, V2700 Oph, KZ Psc and V969 Mon are such stars. Since these stars appear in giant region on the HR diagram and giant stars often tend to have much longer periods, finding such short periods is not expected. One possible explanation is that these stars are likely members of a binary system. IZ Cet and V1330 Tau are such stars among our sample, which are reported as SB2 binaries (Torres et al. 2002). On the other hand, we carried out a quick inspection of space photometry provided by the *TESS* satellite (Ricker et al. 2014) and did not notice any eclipse event for any star in our sample. Unfortunately, we have no high-resolution spectra to check if these stars exhibit an orbital motion in their radial velocities. Another possible explanation is that, if these giants are single, then they might be FK Com variables. These systems deserve additional attention by further spectroscopic studies.

Computing photometric periods and relative shear values for each star enables us to investigate the relation between the photometric period and the relative shear (i.e., differential rotation, Figure 4) via a more extended sample compared to Özdarcan (2021). In the figure, the distribution of the main sequence and giant stars shows a significant distinction

in the shorter periods, while the distinction tends to disappear towards long periods. The slopes of the best-fitting linear fits in Figure 4 indicate that the relative shear is more sensitive to the photometric period in giant stars compared to main-sequence stars. That picture confirms the distinction reported in Özdarcan (2021). Yet, the number of main sequence stars still requires to be increased, particularly for the shorter photometric periods for more reliable results. On the other hand, the distinction between giant and main sequence stars appears to be lost towards the longer photometric periods. Increasing the sample size of main sequence stars having long term continuous photometry is crucial for revealing the true form of the observed distinction between main sequence and giant stars. It is also desirable to observe main sequence stars with short photometric periods that appear below the dashed line in Figure 4). We may argue that these stars show less shear than the relation for longer period MS stars would predict.

In Figure 4, plotting the main sequence stars mentioned in Donahue et al. (1996) together with the target stars analysed in this study might be questionable because Donahue et al. (1996) obtained periods via the S index, which is a chromospheric indicator of the stellar activity, while we use pure V photometry (a photospheric indicator of the same phenomenon) to obtain periods. If the differential rotations of the photosphere and the chromosphere are significantly different from each other, then it is a reasonable concern. Since there are no long-term and simultaneous period measurements of the photosphere and the chromosphere of any star, we can only inspect the rotational behaviour of the solar photosphere and chromosphere and make interpretations in the scope of a solar-stellar connection. In a recent study, Xu et al. (2020) found that rotation periods indicated by chromospheric and photospheric indices vary in the same period range in the Sun (see Figure 6 in their study). This means that the differential rotation of the chromosphere of the Sun is not significantly different from the photosphere. A very recent study by Mishra et al. (2024) reported a 1.59% difference between the equatorial periods found from differential rotations of the solar photosphere and the chromosphere, which indicates a little difference between their rotations. Considering these findings, we may expect a similar behaviour for the chromospherically active stars in the scope of the Solar-Stellar connection. Then, it is reasonable to expect very little difference for SDR values computed from the S index (chromospheric indicator) and broadband V photometry (photospheric indicator). The difference would likely be within our observational errors.

We note that photometric periods are computed by tracing the rotational modulation signal observed in light curves. These signals are produced by cool surface spots. Rotation periods of these spots may be different depending on their latitudinal position on the surface of the star. This is the basic idea in our analysis. However, it was reported that any change in the area of a surface spot, vanishing and emerging of spots in short time scales at various locations on the surface of the star may alter the measured photometric period (Fekel et al. 2002). Such events show themselves as dramatic changes in the peak-to-peak light curve amplitude over short time scales (days). Even if these effects are in progress, we do not expect a significant change in our results because we determine photometric periods from stable parts of the light curves where the amplitude can be fairly accepted as constant.

Upon comparing the summarized findings with the theoretical computations of Kitchatinov & Rüdiger (1999), we observe that our results support the predicted relation between period and differential rotation. However, the observed distinction between giants and main sequence stars appears to be opposite to the theoretical predictions. According to calculations by Kitchatinov & Rüdiger (1999), giant stars should have stronger differential rotation compared to main-sequence stars. However, Figure 4 suggests the opposite, where the main-sequence stars appear to have stronger differential rotation than the giant stars. Further observational and theoretical studies may be conducted to investigate the source of this contradiction.

Kővári et al. (2017) investigated the relation between the rotation period and SDR in the scope of single and binary stars. They found that SDR weakly depends on the rotation period for of a binary system compared to a single star. We are not in a position to test this finding here since we do not consider single/binary distinction in our study. However, a further detailed investigation, which considers binarity and evolutionary status, might yield results that would provide a more comprehensive view of the relation between the SDR and the photometric period for chromospherically active stars.

We are indebted to Dr. Grzegorz Pojmański for providing reduced and unpublished photometric data of target stars from the ASAS3-N and ASAS4 surveys. These data significantly increased the reliability of the results obtained in this study. We also

TABLE 5

ANALYSIS RESULTS OF SEASONAL LIGHT CURVES*

TYC 05275-00646-1 — IM Cet								
HJD begin (24 00000+)	HJD end (24 00000+)	HJD mean (24 00000+)	P_{phot} (day)	σ_P (day)	V_{max} (mag)	V_{min} (mag)	V_{mean} (mag)	N
51868.5706	51931.5318	51900.0512	28.54	0.960	9.995	10.209	10.102	17
52039.9296	52262.5831	52151.2564	28.14	0.200	10.054	10.188	10.121	62
52439.8937	52563.679	52501.7864	28.58	0.210	10.106	10.430	10.268	35
52623.5446	52677.5206	52650.5326	27.96	1.380	10.106	10.474	10.290	17
52787.9123	53035.5455	52911.7289	28.55	0.130	10.098	10.438	10.268	62
53512.9328	53765.5344	53639.2336	28.06	0.100	10.151	10.487	10.319	59
53900.9278	54146.7157	54023.8218	27.97	0.120	10.086	10.344	10.215	52
54246.9291	54498.5336	54372.7314	27.43	0.160	10.172	10.413	10.292	72
54632.9086	54875.7108	54754.3097	28.46	0.140	10.107	10.437	10.272	60
54969.9312	55239.7217	55104.8265	28.19	0.130	10.142	10.584	10.363	99
55367.108	55601.7162	55484.4121	27.83	0.140	10.166	10.599	10.383	165
55696.9278	55969.7267	55833.3273	27.66	0.170	10.264	10.429	10.347	190
56127.0973	56328.7437	56227.9205	28.26	0.300	10.219	10.461	10.340	90
56427.9281	56676.756	56552.3421	28.01	0.130	10.140	10.437	10.289	194
56816.1142	57060.5301	56938.3222	28.08	0.100	10.038	10.290	10.164	211
57154.9277	57424.5312	57289.7295	28.15	0.050	9.955	10.357	10.156	272
57523.9064	57788.7204	57656.3134	28.06	0.090	9.953	10.300	10.127	347
57907.9044	58151.5406	58029.7225	28.36	0.150	9.910	10.194	10.052	264
58256.9314	58511.5387	58384.2351	28.98	0.300	9.910	10.057	9.983	243
58617.9279	58818.5378	58718.2329	29.00	0.700	9.903	10.056	9.979	72
52054.9387	52214.7281	52134.8334	16.91	0.150	11.327	11.527	11.427	28
52453.8408	52578.7414	52516.2911	16.99	0.440	11.324	11.448	11.386	22
52629.5971	52688.5164	52659.0568	17.00	0.320	11.301	11.452	11.376	21
52805.9047	53054.5124	52930.2086	17.19	0.060	11.339	11.508	11.424	70
53525.9300	53780.5195	53653.2248	17.26	0.060	11.307	11.499	11.403	60
53930.1083	54153.7105	54041.9094	16.68	0.130	11.352	11.429	11.391	45
54270.1206	54387.8141	54328.9674	17.27	0.300	11.347	11.473	11.410	46
54399.6743	54509.5175	54454.5959	17.31	0.190	11.304	11.453	11.378	37

*The full table can be viewed online in `https://www.astroscu.unam.mx/rmaa/RMxAA..60-2/PDF/RMxAA..60-2_oozdarcan-VIII-Table5.pdf`.

thank the anonymous referee for thoughtful comments and a critically reading that improved the quality of the manuscript. We acknowledge the Unit of Scientific Research Projects (BAP) at Ege University, for supporting this work through Grant No. 24150.

APPENDICES

A. TRANSFORMATION COEFFICIENTS FOR THE EUOARC OBSERVING SETUP

Equations A1 and A2 are for the EUOARC Johnson measurements for 27th December, 2022 and 13th July, 2023 nights, respectively. $(u-b)_0$, $(b-v)_0$, and v_0 denote reduced instrumental colours and magnitudes.

$$\begin{aligned} V-v_0 &= -0.017(\pm0.045)\times(B-V)+18.648(\pm0.033) \\ B-V &= 1.149(\pm0.016)\times(b-v)_0+0.537(\pm0.006) \\ U-B &= 0.995(\pm0.023)\times(u-b)_0-2.048(\pm0.056) \end{aligned} \tag{A1}$$

$$\begin{aligned} V-v_0 &= -0.059(\pm0.068)\times(B-V)+17.850(\pm0.055) \\ B-V &= 1.020(\pm0.046)\times(b-v)_0+0.533(\pm0.022) \\ U-B &= 1.022(\pm0.074)\times(u-b)_0-1.174(\pm0.121) \end{aligned} \tag{A2}$$

B. SEASONAL LIGHT CURVE ANALYSIS RESULTS

In this section, we tabulate analysis results of seasonal light curves. In the first three columns, begin, end and mean times of each subset are given in heliocentric Julian date. The last column shows the number of data for the corresponding subset.

REFERENCES

Amado, P. J. 2003, A&A, 404, 631, https://doi.org/10.1051/0004-6361:20030494

Baliunas, S. L., Donahue, R. A., Soon, W., & Henry, G. W. 1998, ASPC 154, The Tenth Cambridge Workshop on Cool Stars, Stellar Systems and the Sun, ed. R. A. Donahue & J. A. Bookbinder, 153

Baliunas, S. L., Donahue, R. A., Soon, W. H., et al. 1995, ApJ, 438, 269, https://doi.org/10.1086/175072

Berdnikov, L. N. & Pastukhova, E. N. 2008, PZ, 28, 9

Bernhard, K., Bernhard, C., & Bernhard, M. 2009, OEJV, 98, 1

Bernhard, K. & Lloyd, C. 2008a, OEJV, 92, 1

_____. 2008b, OEJV, 82, 1

Bernhard, K., Lloyd, C., & Frank, P. 2010, OEJV, 123, 1

Bernhard, K. & Otero, S. 2011, PZP, 11, 15

Bressan, A., Marigo, P., Girardi, L., et al. 2012, MNRAS, 427, 127, https://doi.org/10.1111/j.1365-2966.2012.21948.x

Donahue, R. A., Saar, S. H., & Baliunas, S. L. 1996, ApJ, 466, 384, https://doi.org/10.1086/177517

Drilling, J. S. & Landolt, A. U. 2000, in Allen's Astrophysical Quantities, ed. A. N. Cox, 381

Duncan, D. K., Vaughan, A. H., Wilson, O. C., et al. 1991, ApJS, 76, 383, https://doi.org/10.1086/191572

Fekel, F. C., Henry, G. W., Eaton, J. A., Sperauskas, J., & Hall, D. S. 2002, AJ, 124, 1064, https://doi.org/10.1086/341612

Gaia Collaboration, Prusti, T., de Bruijne, J. H. J., et al. 2016, A&A, 595, 1, https://doi.org/10.1051/0004-6361/201629272

Gaia Collaboration, Vallenari, A., Brown, A. G. A., et al. 2023, A&A, 674, 1, https://doi.org/10.1051/0004-6361/202243940

Gray, D. F. 2005, The Observation and Analysis of Stellar Photospheres (CUP), https://doi.org/10.1017/CBO9781316036570

Hardie, R. H. 1964, in Astronomical techniques, ed. W. A. Hiltner, 178

Henden, A. A., Levine, S., Terrell, D., & Welch, D. L. 2015, AAS, 225, 336.16

Høg, E., Fabricius, C., Makarov, V. V., et al. 2000, A&A, 355, 27

Kitchatinov, L. L. & Rüdiger, G. 1999, A&A, 344, 911

Kochanek, C. S., Shappee, B. J., Stanek, K. Z., et al. 2017, PASP, 129, 4502, https://doi.org/10.1088/1538-3873/aa80d9

Kővári, Z., Oláh, K., Kriskovics, L., et al. 2017, AN, 338, 903, https://doi.org/10.1002/asna.201713400

Landolt, A. U. 2009, AJ, 137, 4186, https://doi.org/10.1088/0004-6256/137/5/4186

_____. 2013, AJ, 146, 131, https://doi.org/10.1088/0004-6256/146/5/131

Messina, S. & Guinan, E. F. 2003, A&A, 409, 1017, https://doi.org/10.1051/0004-6361:20031161

Mishra, D. K., Routh, S., Jha, B. K., et al. 2024, ApJ, 961, 40, https://doi.org/10.3847/1538-4357/ad1188

Özdarcan, O. 2021, PASA, 38, 27, https://doi.org/10.1017/pasa.2021.21

Özdarcan, O. & Dal, H. A. 2018, AN, 339, 277, https://doi.org/10.1002/asna.201813391

Özdarcan, O., Evren, S., & Henry, G. W. 2012, AN, 333, 138, https://doi.org/10.1002/asna.201111646

Özdarcan, O., Evren, S., Strassmeier, K. G., Granzer, T., & Henry, G. W. 2010, AN, 331, 794, https://doi.org/10.1002/asna.201011413

Pojmanski, G. 1997, AcA, 47, 467, https://doi.org/10.48550/arXiv.astro-ph/9712146

_____. 2002, AcA, 52, 397, https://doi.org/10.48550/arXiv.astro-ph/0210283

Pojmanski, G., Pilecki, B., & Szczygiel, D. 2005, AcA, 55, 275, https://doi.org/10.48550/arXiv.astro-ph/0508017

Reinhold, T. & Gizon, L. 2015, A&A, 583, 65, https://doi.org/10.1051/0004-6361/201526216

Ricker, G. R., Winn, J. N., Vanderspek, R., et al. 2014, JATIS, 1, 014003, https://doi.org/10.1117/1.JATIS.1.1.014003

Schirmer, J., Bernhard, K., & Lloyd, C. 2009, OEJV, 105, 1

Schlafly, E. F. & Finkbeiner, D. P. 2011, ApJ, 737, 103, https://doi.org/10.1088/0004-637X/737/2/103

Schwarzenberg-Czerny, A. 1991, MNRAS, 253, 198, https://doi.org/10.1093/mnras/253.2.198

_____. 1996, ApJ, 460, 107, https://doi.org/10.1086/309985

Shappee, B. J., Prieto, J. L., Grupe, D., et al. 2014, ApJ, 788, 48, https://doi.org/10.1088/0004-637X/788/1/48

Torres, G., Neuhäuser, R., & Guenther, E. W. 2002, AJ, 123, 1701, https://doi.org/10.1086/3391778

Vaughan, A. H., Preston, G. W., & Wilson, O. C. 1978, PASP, 90, 267, https://doi.org/10.1086/130324

Wilson, O. C. 1978, ApJ, 226, 379, https://doi.org/10.1086/156618

Xu, J.-C., Gao, P.-X., & Shi, X.-J. 2020, ApJ, 902, 64, https://doi.org/10.3847/1538-4357/abb5b7

O. Özdarcan, H. A. Dal, E. Sipahi Kılıç, and E. Yoldaş: Ege University, Faculty of Sciences, Department of Astronomy and Space Sciences, 35100 Bornova, İzmir, Turkey.